Electronic Supplementary Material (ESI) for

Solution-phase process of g-C_3N_4/$BiVO_4$ dyad to large-area photoanode: interfacial synergy for highly efficient water oxidation

Bing Zhang, Shu-Yu Zhao, Tian-Jian Zhao, Hong-Hui Wang, Yong-Xing Liu, Li-Bing Lv, Xiao Wei, Xin-Hao Li *, and Jie-Sheng Chen *

School of Chemistry and Chemical Engineering, Shanghai Jiao Tong University
Shanghai 200240 (P. R. China)

Corresponding authors: xinhaoli@sjtu.edu.cn; chemcj@sjtu.edu.cn

Experimental Procedures

Materials

F-doped SnO_2 (FTO) transparent substrate electrode (Nippon Sheet Glass, Japan, sodalime, sheet resistance: 14 Ω sq^{-1}), cyanamide (Stru Chem Co., Ltd, 95%), sodium sulfate (Adamas, 99%), silver nitrate (Adamas, 99%), bismuth nitrate, ammonium metavanadate, phosphate buffer powder, concentrated nitric acid (65 wt.%), ethanol and acetone were all purchased from Sinopharm Chemical Reagent Co., Ltd and used as received.

Synthesis of the colloidal soltuion of flexible g-C_3N_4 nanolayers

Carbon nitride solids were prepared via thermal condensation of cyanamide at 550 °C in a covered crucible in air. Then 0.1 g of carbon nitride powder was dispersed into 10 mL of HNO_3 (10 N) under stir. The dispersion was heated to 80 °C for 3h. The as-obtained solution was used as such after naturally cooled to room temperature.

Preparation of FTO slides

FTO slides were cut into small pieces with certain area and then washed three times with distilled water, ethanol and acetone successively. The clean FTO slides were kept in distilled water for further use.

Fabrication of pristine g-C_3N_4 electrodes

FTO slides were dipped into the colloidal soltuion of flexible g-C_3N_4 nanolayers for 5 s and then dried at room temperature. The coated slides were then annealed at 400 °C for 2 h.

Typical synthesis of pristine $BiVO_4$ electrodes

Clean FTO slides were dipped into an aqueous solution of 0.1 M $Bi(NO_3)_3{\cdot}5H_2O$, 0.1 M NH_4VO_3 and 2M nitric acid solution for 5 s and then dried at room temperature. The coated slides were then annealed at 400 °C for 2 h in air, resulting in yellow $BiVO_4$ thin films for further characterizations and applications.

Synthesis of $BiVO_4$/g-C_3N_4 electrodes

equal mol of $Bi(NO_3)_3{\cdot}5H_2O$ and NH_4VO_3 were dissolved in 2M aqueous nitric acid solution repespectively, then mixed to form 0.2 M precursor. The concentrated nitric acid (65 wt.%) processed g-C_3N_4 dispersion solution was diluted to certain concentration by which can be equally mixed with $BiVO_4$ precursor solution to form BV/CN-x precursors (x means mol ratios of $BiVO_4$ to g-C_3N_4, here are 2, 5 and 10 respectively). Washed FTO slides with certain area were dipped in the precursor solution for 5 s, after dryness at room temperature, films were calcinated at 400 °C for 2 h in air to form a yellow thin film. Ag^+ doped BV/CN-5 photoanode was prepared by simply immersing the as-obtained BV/CN-5 photoanode in 0.01 M $AgNO_3$ aqueous solution overnight in dark. For the synthesis of $BiVO_4$/bulk g-C_3N_4 (BV/BCN) electrodes, bulk g-C_3N_4 powders without nitric acid processing were directly mixed with $BiVO_4$ precursor, then FTO slides with certain area were dipped in the precursor solution for 5 s, after dryness at room temperature, films were calcinated at 400 °C for 2 h in air.

Photoelectrochemical measurements

The PEC performances were investigated using a three-electrode electrochemical quartz cell in a 0.5 M Na_2SO_4 phosphate buffer solution (pH = 6.8) under simulated sunlight illumination (Perfectlight Tech. Co., Ltd., PLS-SXE300C, 300 W Xe lamp) with a glass optical filter used to cut off the short wavelength part (λ < 400 nm). The light intensity was calibrated using a reference Si solar cell (Oriel-91150). The electrolyte was stirred and bubbled with O_2-saturated gas before the measurements. A saturated calomel electrode (SCE) in saturated KCl solution was used as a reference electrode and a Pt coil was used as a counter electrode. The measured potentials versus SCE were all converted to the reversible hydrogen electrode scale according to the Nernst equation. Mott–Schottky Plots was performed in the above 0.5M Na_2SO_4 aqueous solution using typical three-electrode system at an increasing rate of 50 mV/s from -1.5 V to 0.8 V. Surface photovoltage spectroscopy were conducted with a system consisted of a source of monochromatic light, a lock-in amplifier (SR830-DSP) with a light chopper (SR540), a photovoltaic cell, and a computer. A 500 W xenon lamp and a grating monochromator (Omni-λ 500) were combined to provide the monochromatic light. A low chopping frequency of ∼23 Hz was used to obtain stable and intensive signals. The photovoltaic cell was a sandwich-like structure consisting of FTO-sample-FTO. For measuring the incident photon-to-current efficiency (IPCE), the xenon lamp 40 lamp (Newport 67 005) was connected to a Newport monochromator. Two lenses were used to focus monochromatic light onto the active area of the DSSCs. The light output was modulated to certain wavelength and the IPCE data were calibrated with a NREL calibrated reference cell.

Characterizations

The SEM measurements were performed on a FEI Nova NanoSEM 2300. The TEM and HRTEM measurements were taken with a JEM-2100F microscope operated at an acceleration voltage of 200 kV. The AFM tests were conducted with a Nanonavi E-Sweep Scanning Probe Microscope. The Powder X-ray diffraction (XRD) patterns were recorded on a Bruker D8 Advance X-ray diffractometer with Cu-Kα radiation (λ = 1.5418 Å) with a scan rate of 6° min^{-1}. UV-vis spectra were taken with a SHIMADZU UV-2450 UV-vis spectrophotometer.

Results and Discussion

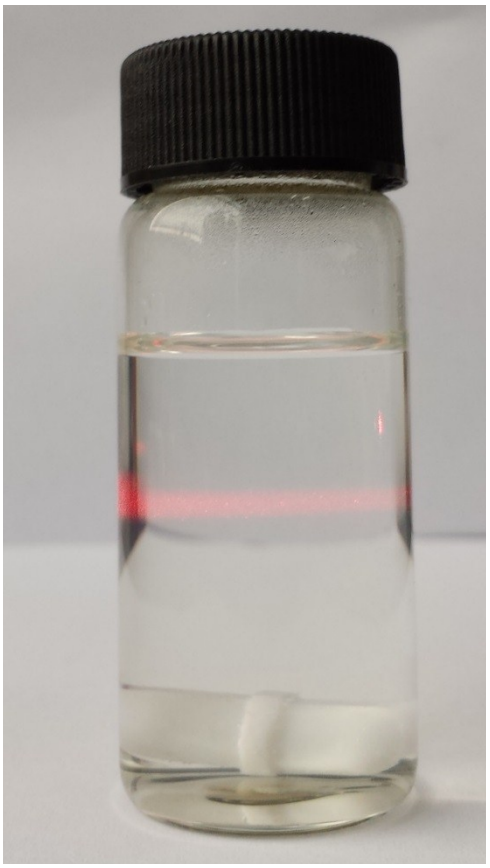

Figure S1. Photograph of the aqueous dispersion of g-C_3N_4 nanolayers for the fabrication of BV/CN photoanodes. The typical Tyndall effect well illustrated the nature of colloidal solution.

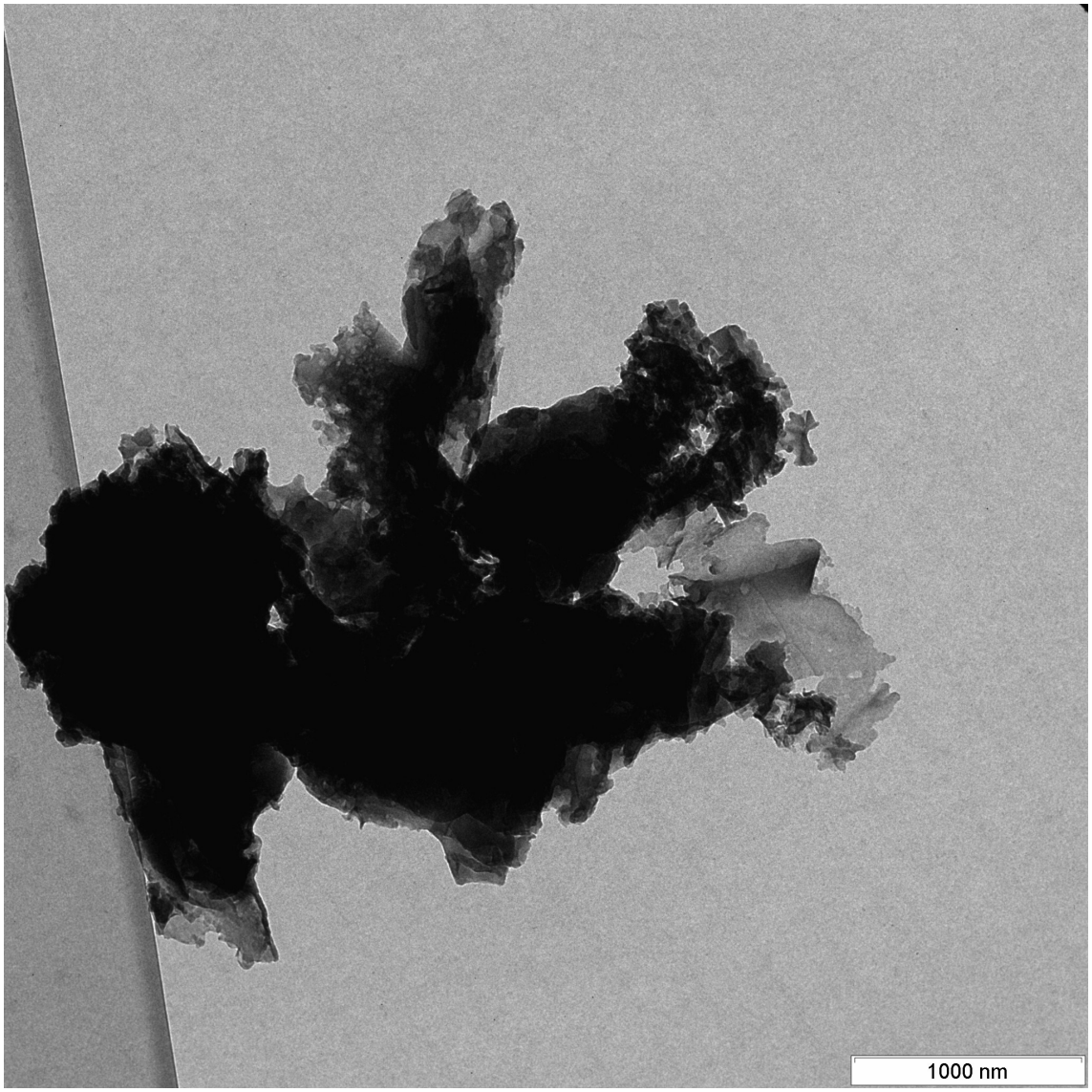

Figure S2. TEM image of g-C_3N_4 before exfoliation. The irregular shape of condensed g-C_3N_4 solid can be clearly seen.

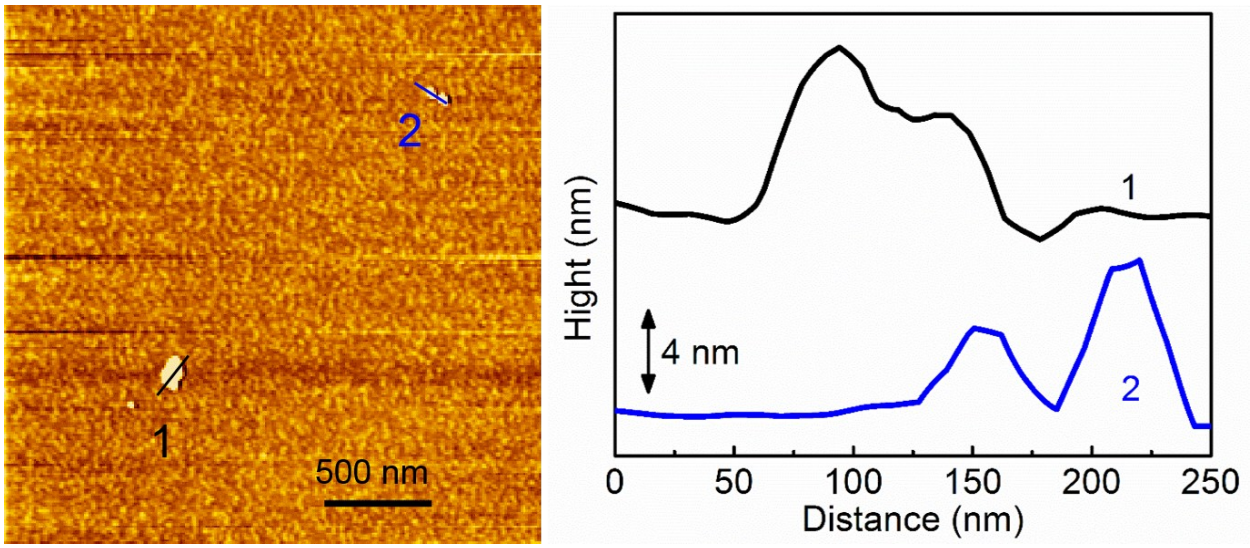

Figure S3. AFM image of g-C_3N_4 nanosheets in the g-C_3N_4 aqueous dispersion. The thickness of as-exfoliated g-C_3N_4 nanolayers was around 4-8 nm.

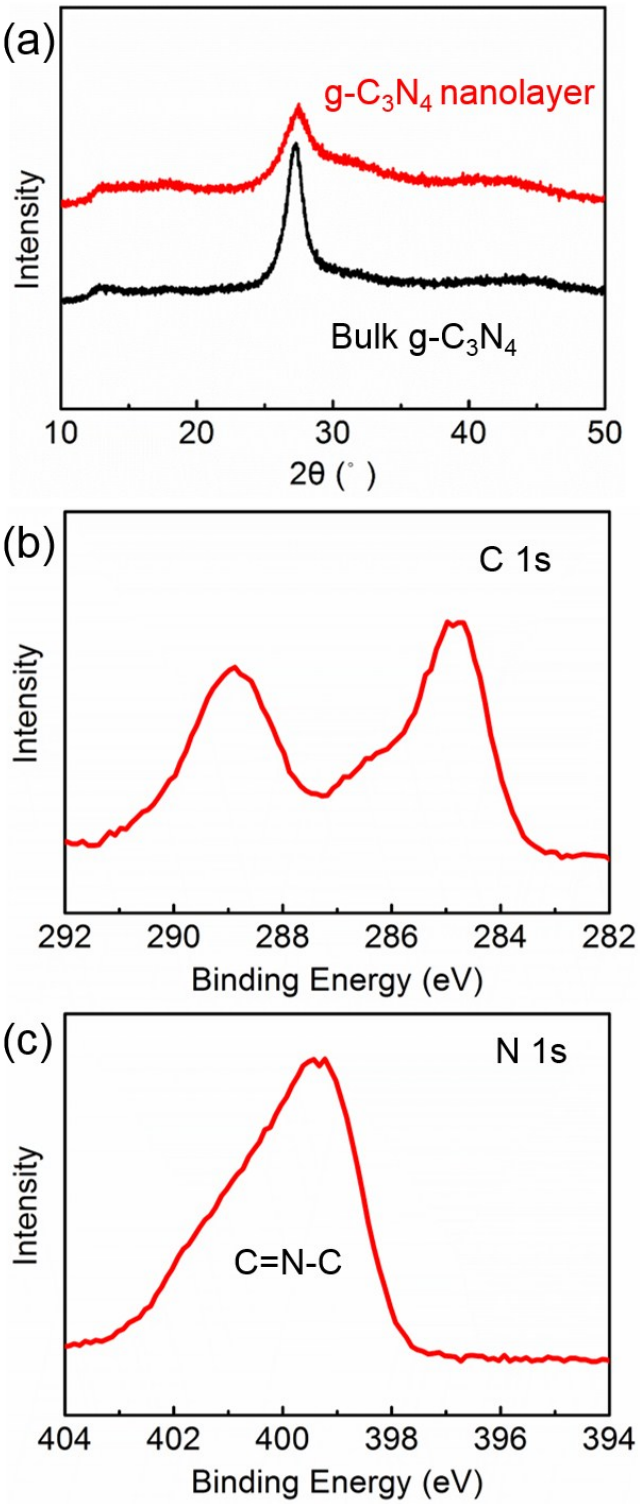

Figure S4. XRD patterns of g-C_3N_4 powder samples (a) and XPS spectra of g-C_3N_4 nanolayers (b-c). XRD peaks near 13.1 and 27 illustrated that g-C_3N_4 nanolayers possessed the very nature of bulk g-C_3N_4. C 1s (b) and N 1s (c) XPS spectra also showed typical spectra originated from C and N atoms in the conjugated C=N-N system of triazine. Note that the typical peaks of sp^2 C-C bonds of graphitic carbon at 284.6 eV, which generally existed in all g-C_3N_4 samples in the literature [S1].

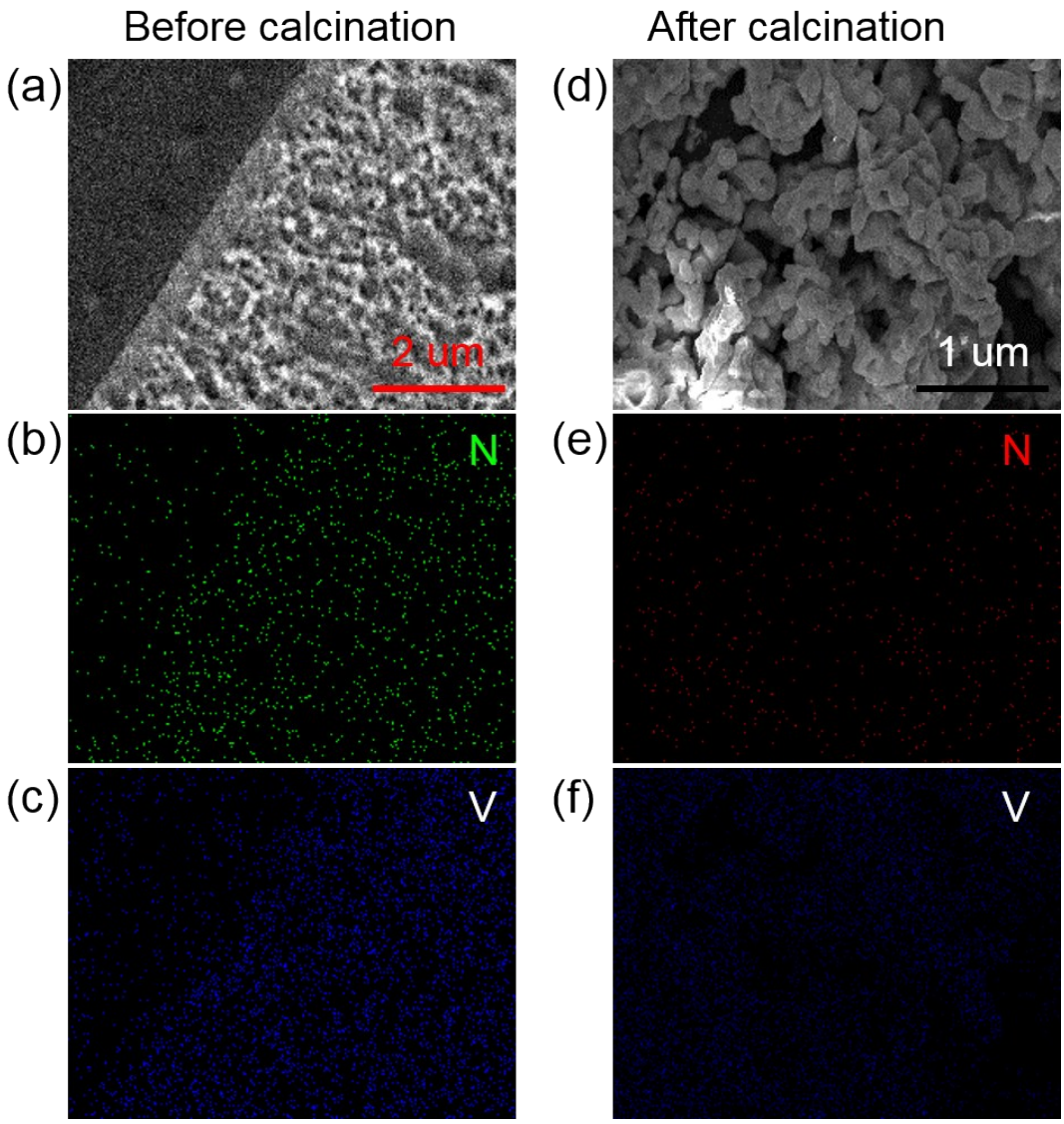

Figure S5. SEM image and element distribution of BV/CN-5 precursor dried at room temperature. The well dispersed g-C_3N_4 nanolayers revealed the supramolecular assembly of highly dispersed g-C_3N_4 nanolayers with the chains of $[VO_3]_n^-$ into uniform foam-like thin films (a-c). After calcination at 400 °C (d-f), monoclinic $BiVO_4$ nanocrystals[17] and BV/CN nanocomposites formed. Elemental mapping results demonstrated the well dispersion of g-C_3N_4 nanolayers and $BiVO_4$.

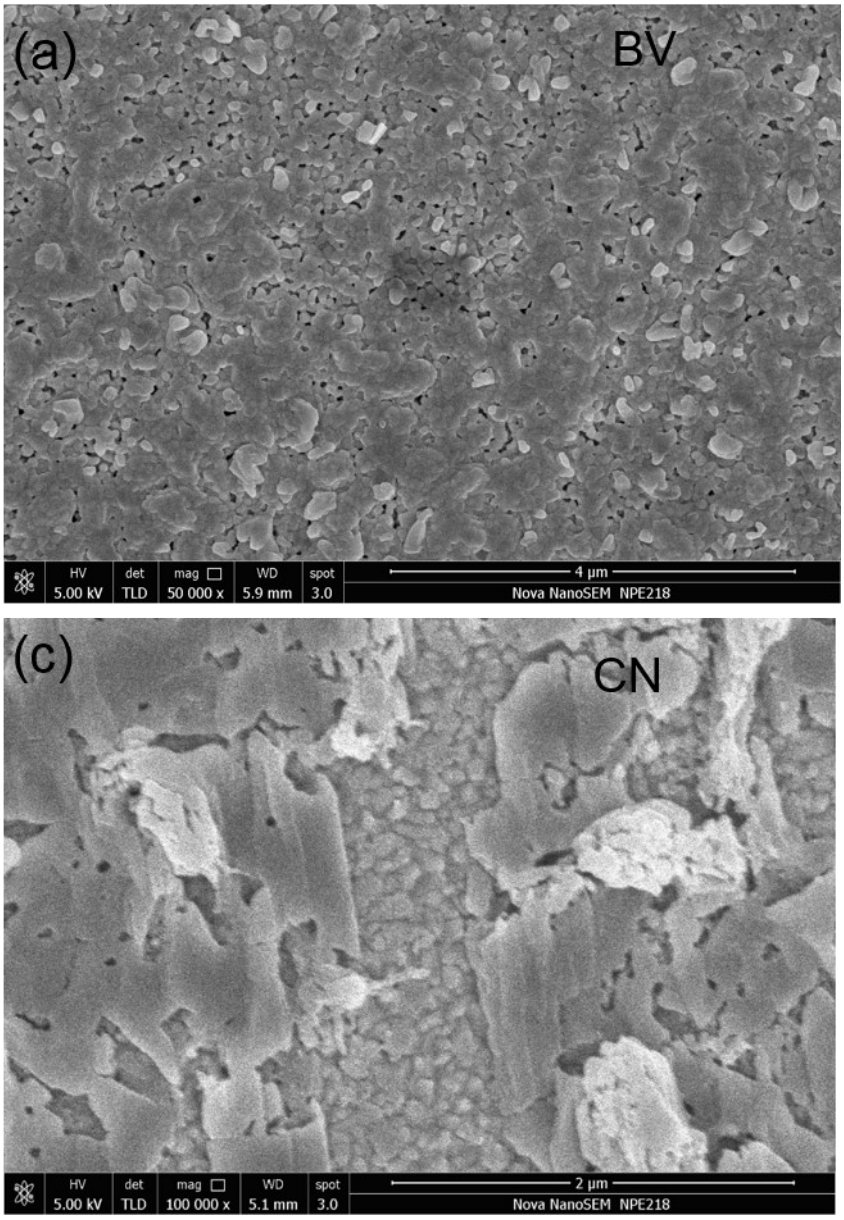

Figure S6. SEM images of pristine $BiVO_4$ and pristine g-C_3N_4 photoanodes. Typical surface of pristine $BiVO_4$ photoanode (a) and g-C_3N_4 photoanode (b) after calcination at 400 ^oC. Pristine $BiVO_4$ photoanode exhibited irregular porous structure and nanocrystals and pristine g-C_3N_4 photoanode showed either irregular large sheets structure. While the introduction of g-C_3N_4 nanolayers can maintain BV/CN-5 photoelectrodes uniform porous structure and nanocrystals. The as-exfoliated g-C_3N_4 nanolayers with a rich amount of -NH_2 groups on the surface or edges could also function as "linkers" to connect the chains of $[VO_3]_n^-$ which helped to ensure the formation of uniform structure.

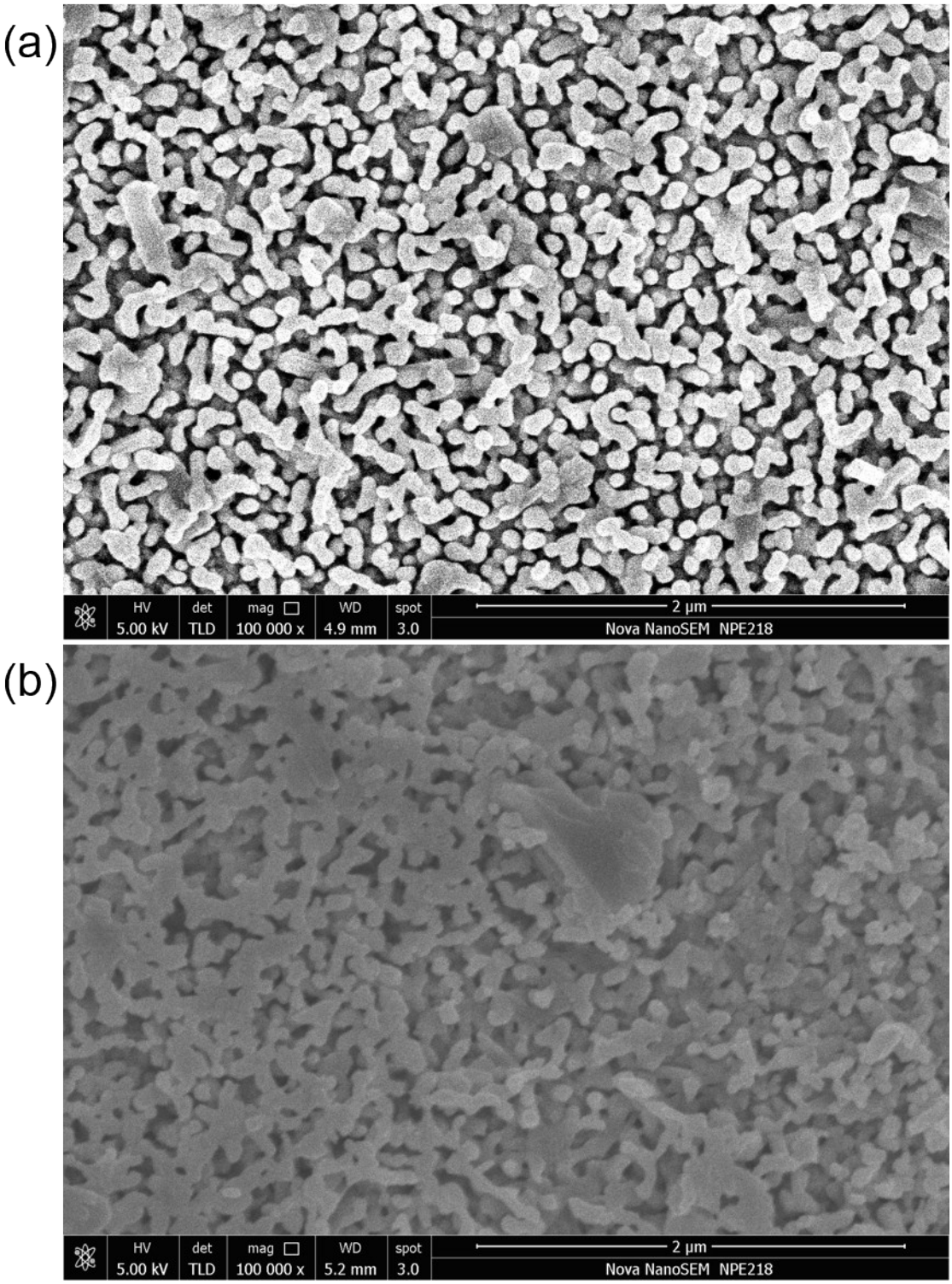

Figure S7. Typical SEM images of BV/CN-2 (a) and BV/CN-10 (b) photoanodes. Relative uniform nanocrystals can be seen in two photoanodes further revealed the "linker" function of g-C_3N_4 nanolayers.

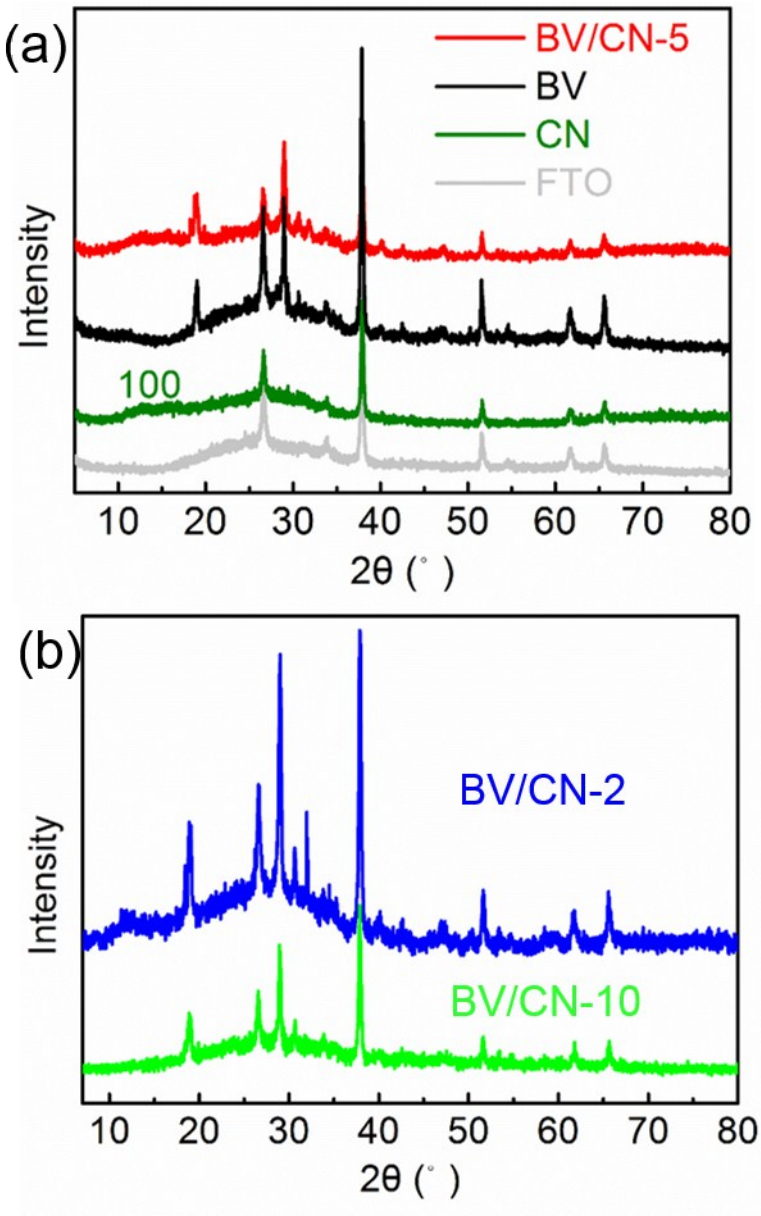

Figure S8. XRD patterns of different photoanodes. Peaks near 13.1 showed the existence of g-C_3N_4 and peaks closing to 29.7 indicated the formation of monoclinic $BiVO_4$ (m-$BiVO_4$). m-$BiVO_4$ was considered as most promising candidates for photo or photoelectrochemical applications among all crystal structures of $BiVO_4$.

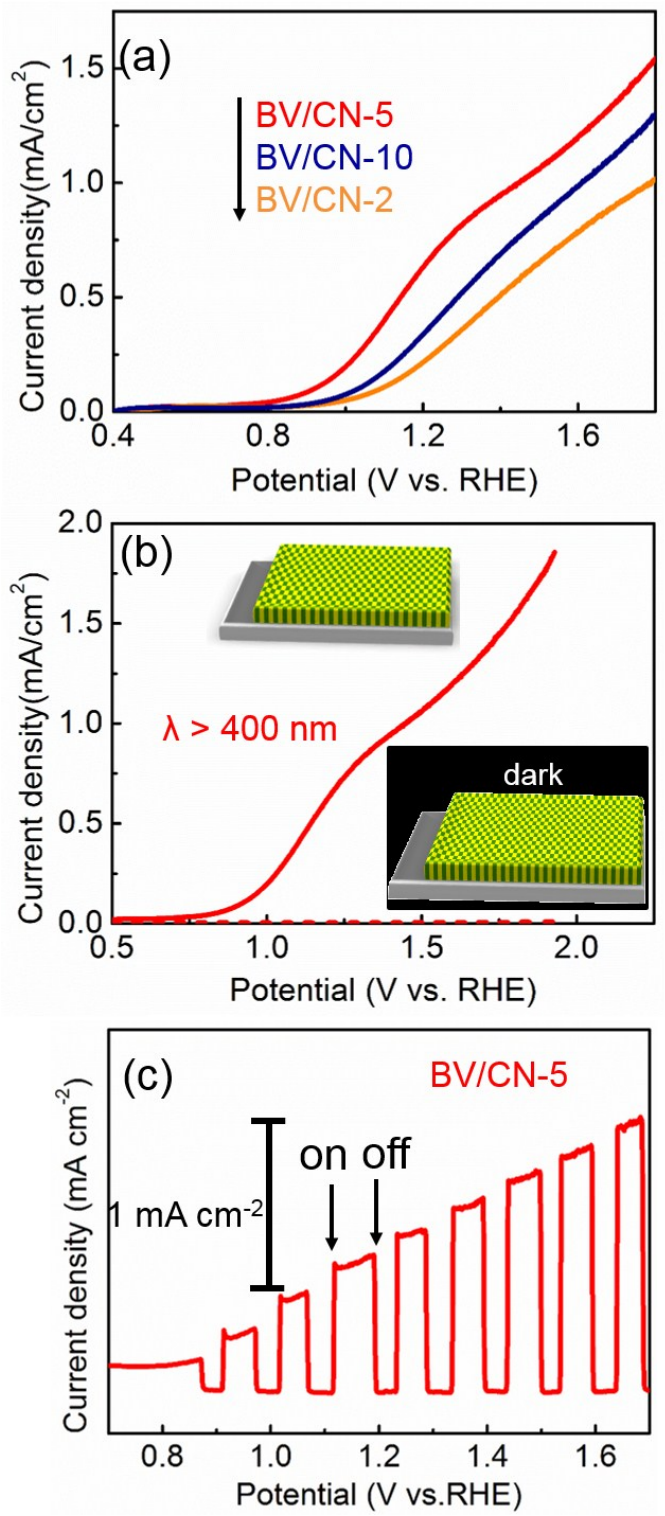

Figure S9. LSV curves of BV/CN photoanodes with different mol ratios for photoelectrochemical OER. (a) LSV curves of BV/CN photoanodes with different mol ratios for photoelectrochemical OER under visible irradiation. BV/CN-5 photoanode exhibited the best photoelectrochemical OER performance. The synergistic effect between g-C_3N_4 and $BiVO_4$ well explained the variation in the current output upon changing the mol ratios of g-C_3N_4 and $BiVO_4$ in dyadic thin films, which largely dominated the photo-excited charge free transfer path and thus final OER performance (b) LSV curves of BV/CN-5 photoanodes for photoelectrochemical OER with visible irradiation or in dark. The chopped *i-V* curve of BV/CN-5 photoanode (c) which showed the same tendency with the linear *i-V* curves also indicated the fast response of the BV/CN-5 electrode to photo illumination in relatively low overpotentials.

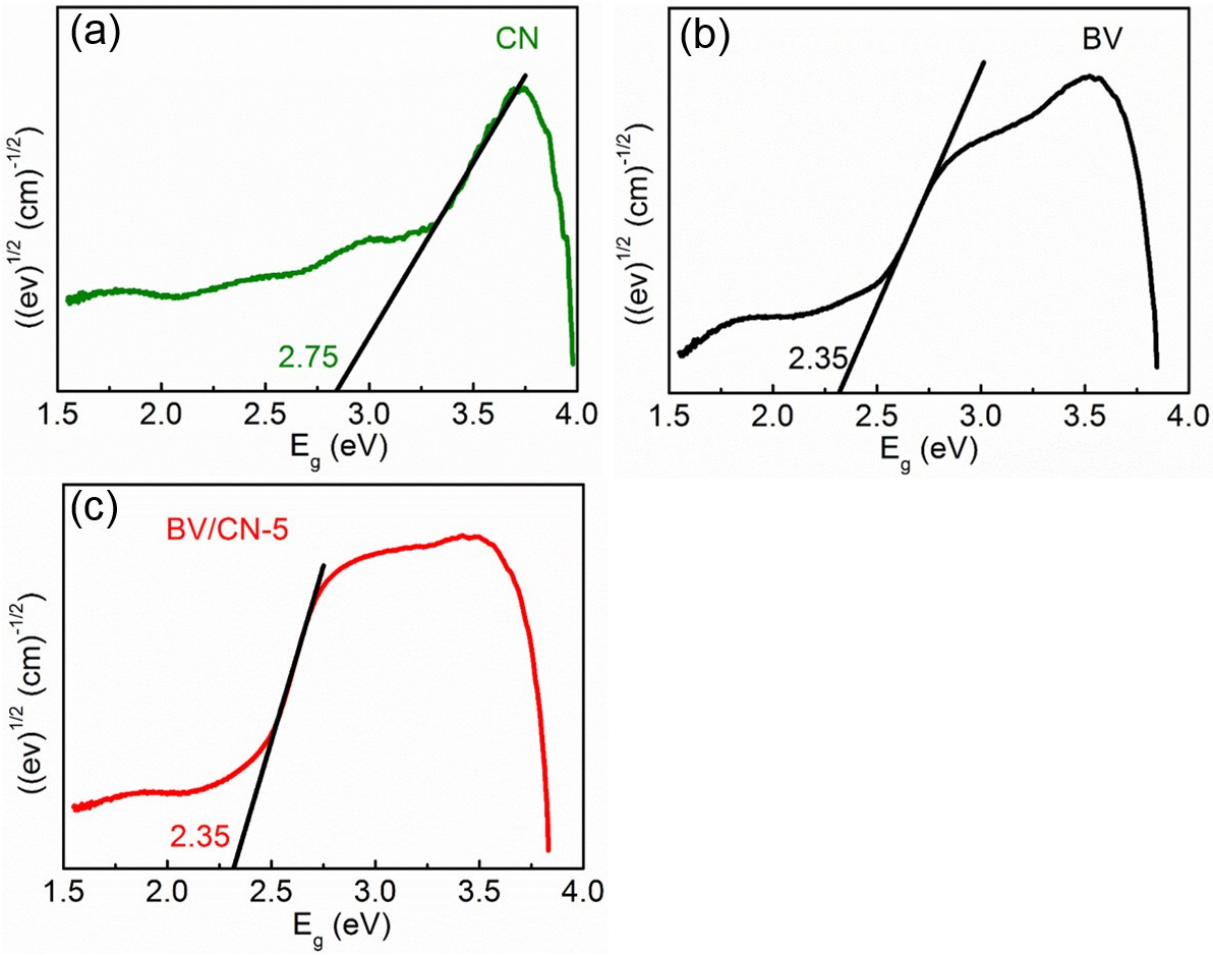

Figure S10. Band gaps of BV/CN-5, pristine $BiVO_4$ and pristine g-C_3N_4 photoanodes calculated according to UV-vis spectrum. The band gap of $BiVO_4$ in BV/CN-5 was not changed compared with pristine $BiVO_4$.

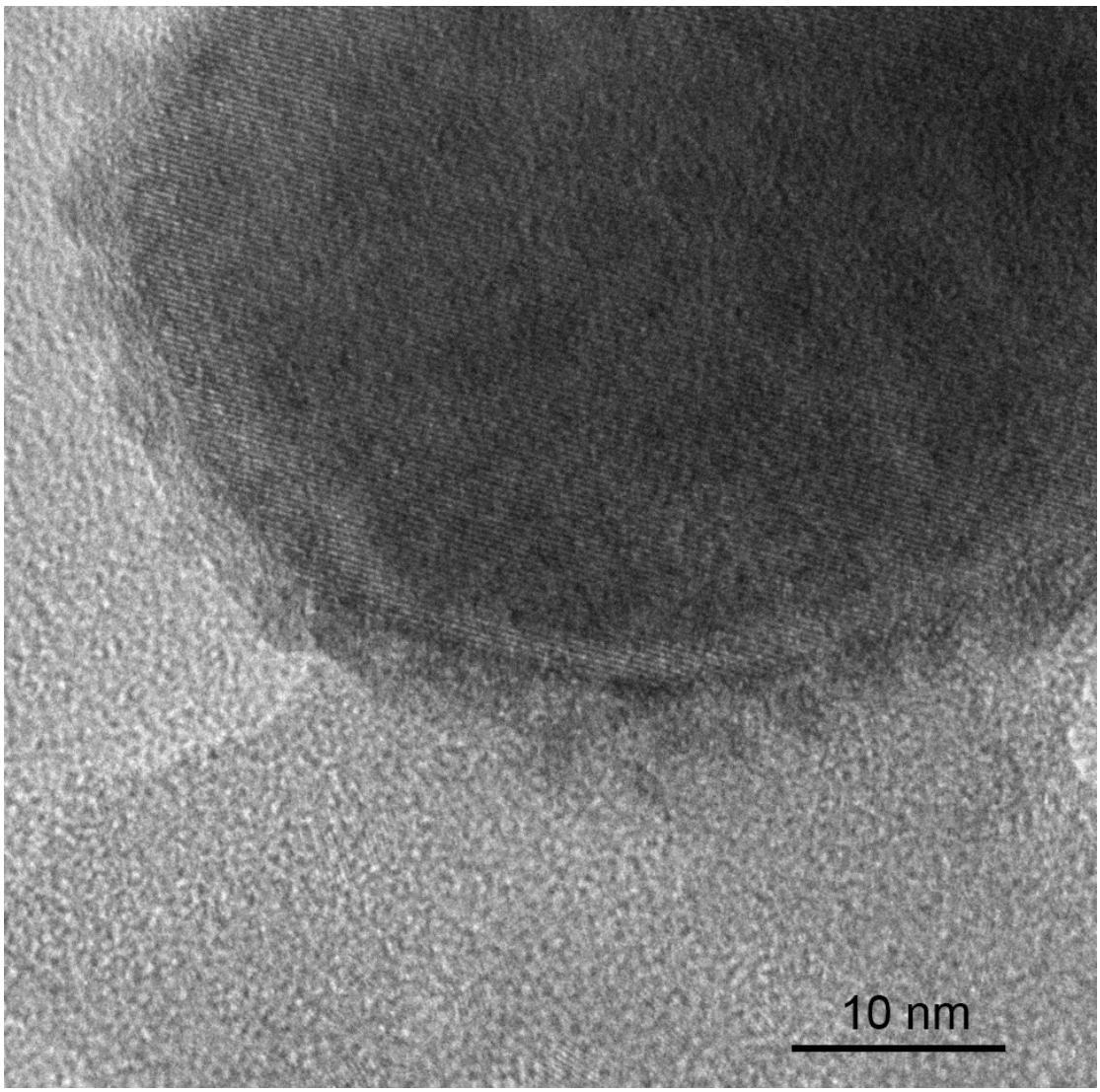

Figure S11. HRTEM image of BV/CN-5 photoanode after calcination. The results revealed the fine structure of composite photoanode and the high crystallinity with clear lattice structures attributed to the (121) facet of the monoclinic phase of $BiVO_4$.

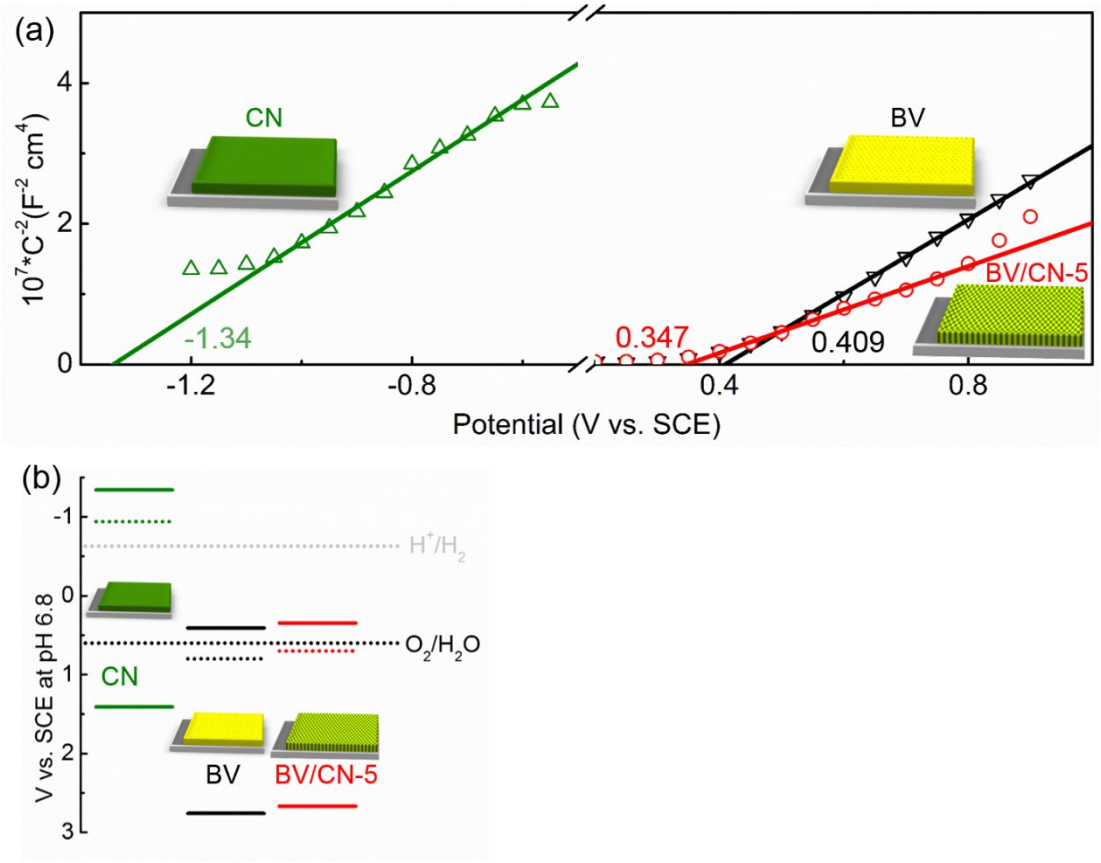

Figure S12. Electronic structure analysis for BV/CN-5, pristine $BiVO_4$ and pristine g-C_3N_4 photoanodes. Mott-schottky curves in 0.5 M Na_2SO_4 solution (a) and corresponding schematic diagram of energy band structure (b) of BV/CN-5, pristine $BiVO_4$ and pristine g-C_3N_4 photoanodes. The valance and conduction band position of BV/CN-5 was slightly elevated due to the introduction of g-C_3N_4 nanolayers, rather suggesting the formation of a rectifying contact between the $BiVO_4$ and g-C_3N_4 components.

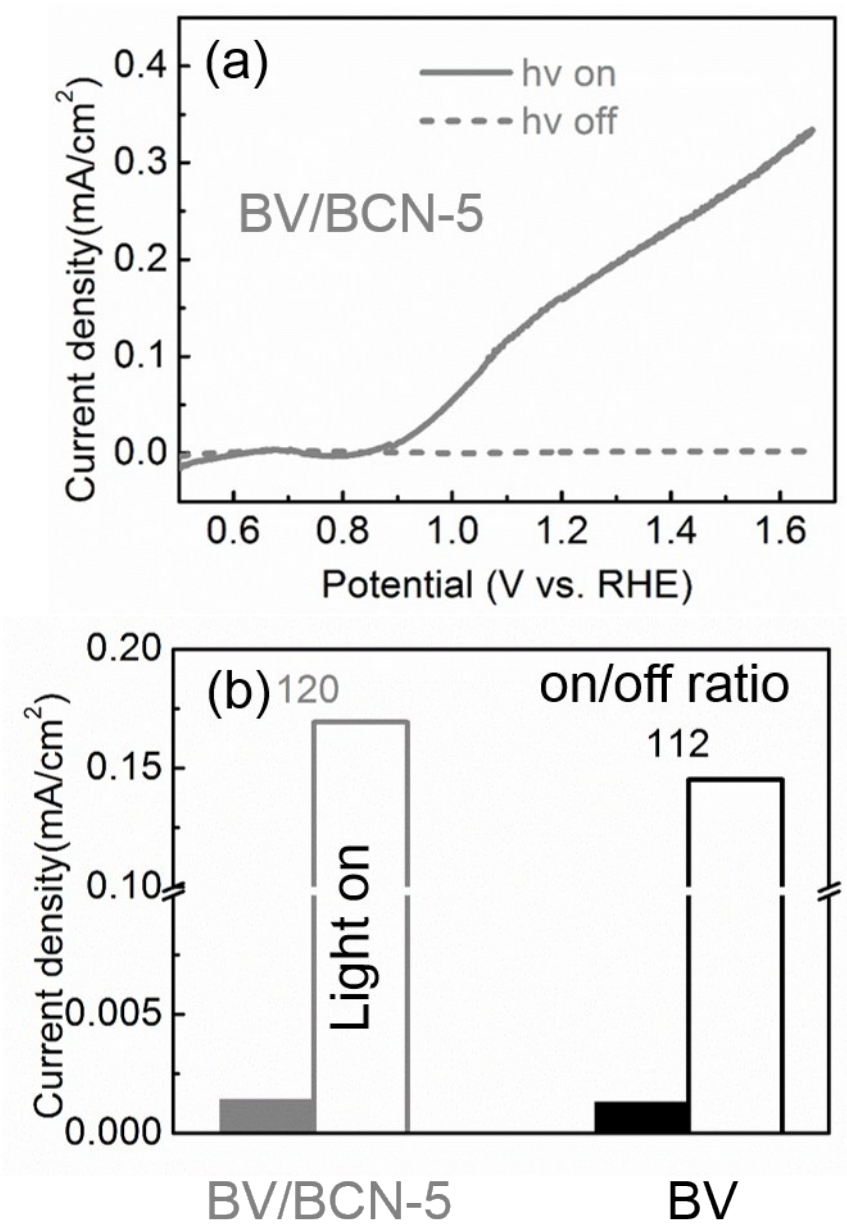

Figure S13. Photoelectrochemical OER performance of $BiVO_4$ and bulk g-C_3N_4 photoanode (BV/BCN-5) in 0.5 M Na_2SO_4 solution. The introduction of bulk g-C_3N_4 with condensed solid structure showed negligible improvement for photoelectrochemical OER compared with pristine $BiVO_4$ photoelectrodes which further illustrated the importance of ultrathin and flexible nature of g-C_3N_4 nanolayers for constructing efficient heterojunctions with $BiVO_4$.

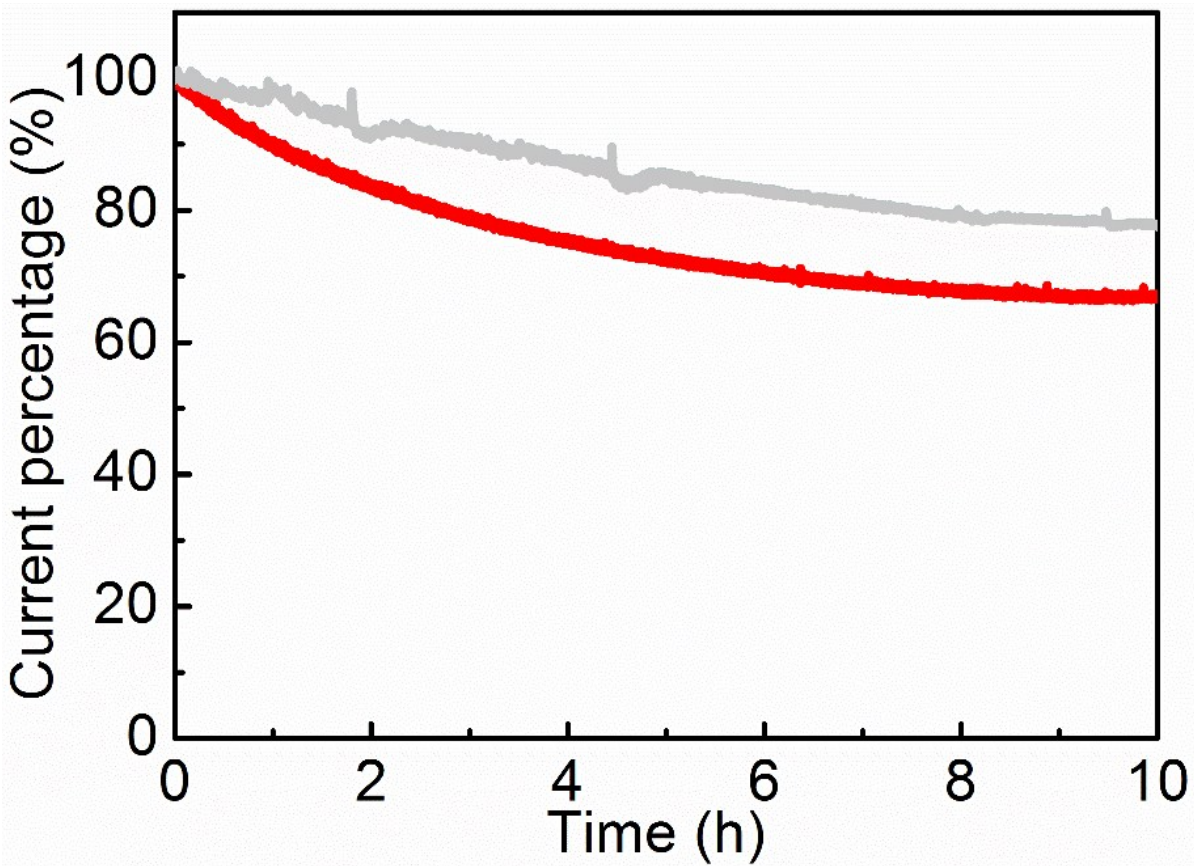

Figure S14. Current-time of BV/CN-5 for photoelectrochemical oxidation with (gray) or without Ag^+ (red) doping in 0.5 M Na_2SO_4 phosphate buffer solution. Ag^+ doped BV/CN-5 photoanodes (Ag^+: BV/CN-5) was proved to further enhance the long-time durability of photoanode with more than 80% catalytic activity reserved after 10 hours' water splitting reaction. This is to say that our method could be extended for further modifying the OER performance via introducing additional dopants and cocatalysts.

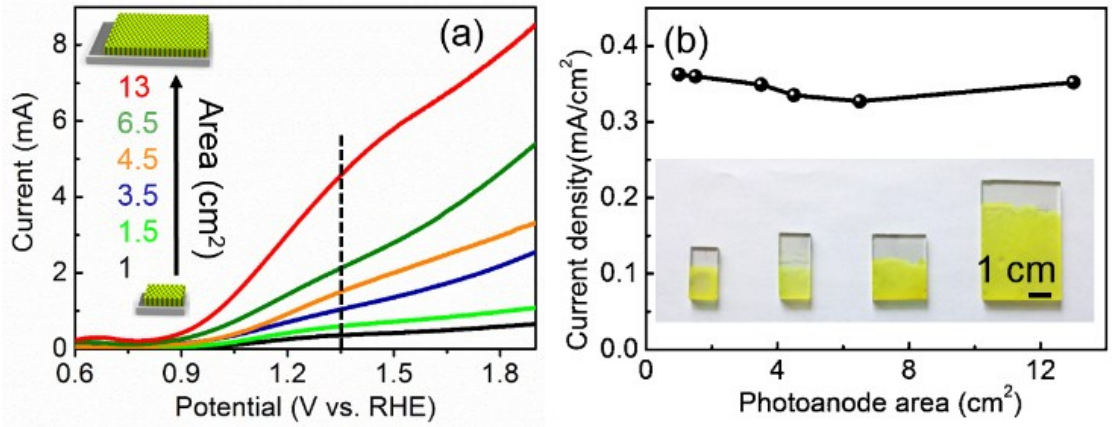

Figure S15. OER performance of scaled-up photoanodes of BV/CN-5 dyad. LSV curves (a) of BV/CN-5 photoanodes for photoelectrochemical OER and corresponding current density (b) at 1.35 V vs. RHE at a distance with 0.3 sun irradiation. Inset b: Photographs of typical BV/CN-5 photoanodes with different areas.

Table S1. IPCE of $BiVO_4$ based photoanodes prepared by solution-phase method for photoelectrochemical water oxidation performance at different voltage

Photoanodes	$IPCE_{\lambda400}$ (%)	Voltage	Ref.
$BiVO_4$-TiO_2	11.5	~1.65 V vs. RHE	S2
$BiVO_4$-WO_3	37.5	~1.3V vs. RHE	S3
Mo:BiVO4	38	1.23 V vs. RHE	S4
SnO_2/$BiVO_4$	30	1.63 vs. RHE	S5
WO_3/$BiVO_4$	31	0.5V bias	S6
Co-Pi/W:$BiVO_4$	32	1.2 V vs. RHE	S7
RhO_2/Mo–$BiVO_4$	~48	1 V vs. RHE	S8
$BiVO_4$/SnO_2/WO_3	43	1.2V vs. RHE	S9
SnO_2/$BiVO_4$:W	49	1.63 vs. RHE	S5
g-C_3N_4/$BiVO_4$	50	1.23 V vs. RHE	This paper
	97	1.6 V vs. RHE	

References

[1] H. Yu, L. Shang, T. Bian, R. Shi, G. I. N. Waterhouse, Y. Zhao, C. Zhou, L.-Z. Wu, C.-H. Tung and T. Zhang, *Adv. Mater.* 2016, **28**, 5080-5086.

[2] S. Ho-Kimura, S. J. A. Moniz, A. D. Handoko and J. Tang, *J. Mater. Chem. A,* 2014, **2**, 3948-3953.

[3] S. J. Hong, S. Lee, J. S. Jang and J. S. Lee, *Energy Environ. Sci.,* 2011, **4**, 1781-1787.

[4] K. P. S. Parmar, H. J. Kang, A. Bist, P. Dua, J. S. Jang and J. S. Lee, *ChemSusChem,* 2012, **5**, 1926-1934.

[5] Y. Liang, T. Tsubota, L. P. A. Mooij and R. van de Krol, *J. Phys. Chem. C,* 2011, **115**, 17594-17598.

[6] J. Su, L. Guo, N. Bao and C. A. Grimes, *Nano Lett.,* 2011, **11**, 1928-1933.

[7] D. K. Zhong, S. Choi and D. R. Gamelin, *J. Am. Chem. Soc.,* 2011, **133**, 18370-18377.

[8] W. Luo, Z. Yang, Z. Li, J. Zhang, J. Liu, Z. Zhao, Z. Wang, S. Yan, T. Yu and Z. Zou, *Energy Environ. Sci.,* 2011, **4**, 4046-4051.

[9] R. Saito, Y. Miseki and K. Sayama, *Chem. Commun.,* 2012, **48**, 3833-3835.